


# Brain parenchymal damage in neuromyelitis optica spectrum disorder – A multimodal MRI study

F. Pache<sup>1,2</sup>  · H. Zimmermann<sup>1</sup> · C. Finke<sup>2,3</sup> · A. Lacheta<sup>1</sup> · S. Papazoglou<sup>1</sup> · J. Kuchling<sup>1</sup> · J. Wuerfel<sup>1</sup> · B. Hamm<sup>4</sup> · K. Ruprecht<sup>2</sup> · F. Paul<sup>1,2</sup> · A. U. Brandt<sup>1</sup> · M. Scheel<sup>1,4</sup>

Received: 3 November 2015 / Revised: 22 January 2016 / Accepted: 11 February 2016 / Published online: 24 March 2016  
© European Society of Radiology 2016

## Abstract

**Objective** To investigate different brain regions for grey (GM) and white matter (WM) damage in a well-defined cohort of neuromyelitis optica spectrum disorder (NMOSD) patients and compare advanced MRI techniques (VBM, Subcortical and cortical analyses (Freesurfer), and DTI) for their ability to detect damage in NMOSD.

**Methods** We analyzed 21 NMOSD patients and 21 age and gender matched control subjects. VBM (GW/WM) and DTI whole brain (TBSS) analyses were performed at different statistical thresholds to reflect different statistical approaches in previous studies. In an automated atlas-based approach, Freesurfer and DTI results were compared between NMOSD and controls.

**Results** DTI TBSS and DTI atlas based analysis demonstrated microstructural impairment only within the optic radiation or in regions associated with the optic radiation (posterior thalamic radiation  $p < 0.001$ , 6.9 % reduction of fractional

anisotropy). VBM demonstrated widespread brain GM and WM reduction, but only at exploratory statistical thresholds, with no differences remaining after correction for multiple comparisons. Freesurfer analysis demonstrated no group differences.

**Conclusion** NMOSD specific parenchymal brain damage is predominantly located in the optic radiation, likely due to a secondary degeneration caused by ON. In comparison, DTI appears to be the most reliable and sensitive technique for brain damage detection in NMOSD.

## Key Points

- *The hypothesis of a widespread brain damage in NMOSD is challenged.*
- *The optic radiation (OR) is the most severely affected region.*
- *OR-affection is likely due to secondary degeneration following optic neuritis.*
- *DTI is currently the most sensitive technique for NMOSD-related brain-damage detection.*
- *DTI is currently the most reliable technique for NMOSD-related brain-damage detection.*

**Electronic supplementary material** The online version of this article (doi:10.1007/s00330-016-4282-x) contains supplementary material, which is available to authorized users.

✉ F. Pache  
florence.pache@charite.de

**Keywords** Diffusion tensor Imaging · Neuromyelitis optica spectrum disorder · Optical coherence tomography · Demyelination · VBM analysis

<sup>1</sup> NeuroCure Clinical Research Center and Experimental and Clinical Research Center, Max Delbrueck Center for Molecular Medicine and Charité- Universitätsmedizin Berlin, Berlin, Germany

<sup>2</sup> Department of Neurology, Charité- Universitätsmedizin Berlin, Berlin, Germany

<sup>3</sup> Berlin School of Mind and Brain, Humboldt-Universitaet zu Berlin, Berlin, Germany

<sup>4</sup> Department of Radiology, Charité- Universitätsmedizin Berlin, Berlin, Germany

## Introduction

In neuromyelitis optica spectrum disorder (NMOSD), conventional brain MRI is typically unremarkable or demonstrates white matter lesions in a subset of patients [1, 2]. Yet, some recent studies using advanced MRI techniques described brain parenchymal damage in normal-appearing white and gray matter (WM and GM). However, these studies provided very

conflicting results regarding the extent, aetiology and clinical implications of this damage [3–24].

NMOSD is a rare autoimmune condition characterized by monophasic or recurrent attacks of optic neuritis (ON) and longitudinal extensive transverse myelitis (LETM), as well as certain forms of area postrema, other brainstem, diencephalic, or certain cerebral presentations [24–26]. For decades, NMOSD was thought to be a variant of multiple sclerosis (MS), but in 2004, a highly specific biomarker was discovered [27] and identified as an antibody targeting aquaporin-4 (AQP-4), an astrocytic water channel [26, 28, 29]. After the discovery of AQP-4, the diagnostic criteria of NMO and its spectrum diseases (NMOSD) were revised in 2006 [30] to include the AQP-4 antibody biomarker. Yet, a second revision just recently took neuroimaging findings into account to enable NMOSD diagnosis when AQP-4 Ab is negative or tests are unavailable [31, 32].

Brain MR imaging shows white matter lesions in about 30–60 % of NMOSD patients [33]. Beside lesions in brainstem, especially located to the area postrema and diencephalon, these lesions are typically small, punctuate and located nonspecifically [34–36], although distribution of lesions may fulfill Barkhof's criteria for MS [1]. Also, in ultra-high field MRI (7 Tesla) NMOSD, white matter lesions appear nonspecific but are distinct from MS lesions [37, 38]. There is a minority of patients (e.g. eight of 120 in a study by Pittock et al. [39]) that show extended lesions in the hypothalamus, periaqueductal grey and area postrema [39, 40]. While the latter lesions may be explained through specific binding of anti-AQP4 antibodies to these regions with a less tight blood–brain-barrier and high AQP-4 expression, the aetiology and significance of unspecific white matter lesions in NMOSD is controversial [34–36]. Moreover, it is debated if and to what extent occult structural brain damage occurs in NMOSD. Several recent studies [3–5, 7–10, 12–16, 19–23, 35, 41–46] using different advanced MRI techniques (proton MR spectroscopy – H-MRS [7–9]; magnetization transfer imaging (MTI) [3, 4, 15]; voxel based morphometry – VBM [16, 20, 22]; subcortical volume and cortical thickness analyses (Freesurfer) [10, 20]; and diffusion tensor imaging (DTI) [5, 6, 11–15, 19, 20] reported conflicting results ranging from: 1) widespread brain damage, 2) damage only in visual and sensorimotor systems, or 3) no substantial damage at all.

Some studies could demonstrate a correlation of MR based measures with clinical scores (visual and motor function) [44] or an objective measure of retinal thinning with optical coherence tomography (OCT) [20].

The overall interpretation of these studies is hampered by the miscellaneous imaging methods, different statistical approaches, and heterogeneous patient cohorts.

Against this background, this multimodal imaging study aimed 1) to investigate different brain regions for GM and WM damage in a well-defined cohort of NMOSD patients,

and 2) to compare three advanced MRI techniques (voxel based morphometry – VBM, subcortical and cortical analyses (Freesurfer), and diffusion tensor imaging - DTI) for their ability to detect non-overt tissue damage in NMOSD.

An association of structural damage in regions with significant group differences and the Expanded Disability Status Scale (EDSS) and disease duration was further explored.

Additionally, to assess potential brain damage related to a history of ON and to correlate MR imaging parameters with clinical scores and OCT measurement, retinal nerve fibre layer thickness (RNFL) was measured.

## Materials and methods

### Study participants

Patients fulfilling diagnostic criteria [30, 31, 47] for NMOSD were prospectively recruited from the outpatient clinics of the NeuroCure Clinical Research Center and at the Department of Neurology, Charité – Universitätsmedizin Berlin. Patients were excluded when presenting with eye or retina diseases other than ON, a refractive error greater than  $\pm 6$  dpt and acute ON or treatment with corticosteroids within three months prior to examination. All study participants gave informed written consent and the study was approved by the local ethics committee.

We initially included 42 NMOSD patients fulfilling the above criteria. To assure a defined non-heterogeneous patient cohort, we excluded 21 patients from the final analysis. We excluded three patients who tested positive for myelin-oligodendrocyte-glycoprotein (MOG-) antibodies, since MOG-ab positive NMOSD is discussed as a different disease, despite having similar phenotype [48]. In addition, 11 patients had to be excluded due to an incomplete MRI exam or insufficient scan quality. Non-Caucasian patients were excluded ( $n=2$ ) due to a potential disease heterogeneity across ethnicities [49]. One patient was excluded due to an unusual white matter lesion of unknown aetiology in the occipital white matter. Considering the high prevalence of unspecific white matter lesions in the elderly population, we included only participants younger than 69 years; therefore, another four NMOSD patients were excluded from the final analysis. Healthy control subjects were selected from the centre's research database matching age and gender. For a flow chart of inclusion/exclusion, see Fig. 1.

### MRI—acquisition and T2 lesion analysis

The multimodal brain MR exam at the same 3 T MRI (Tim TRIO Siemens) included a volumetric high-resolution T1 weighted magnetization prepared rapid acquisition gradient echo (MPRAGE) sequence (TR/TE/TI=1900/2.55/900 ms, FOV=240 x 240 mm<sup>2</sup>, matrix 240 x 240, 176 slices, slice

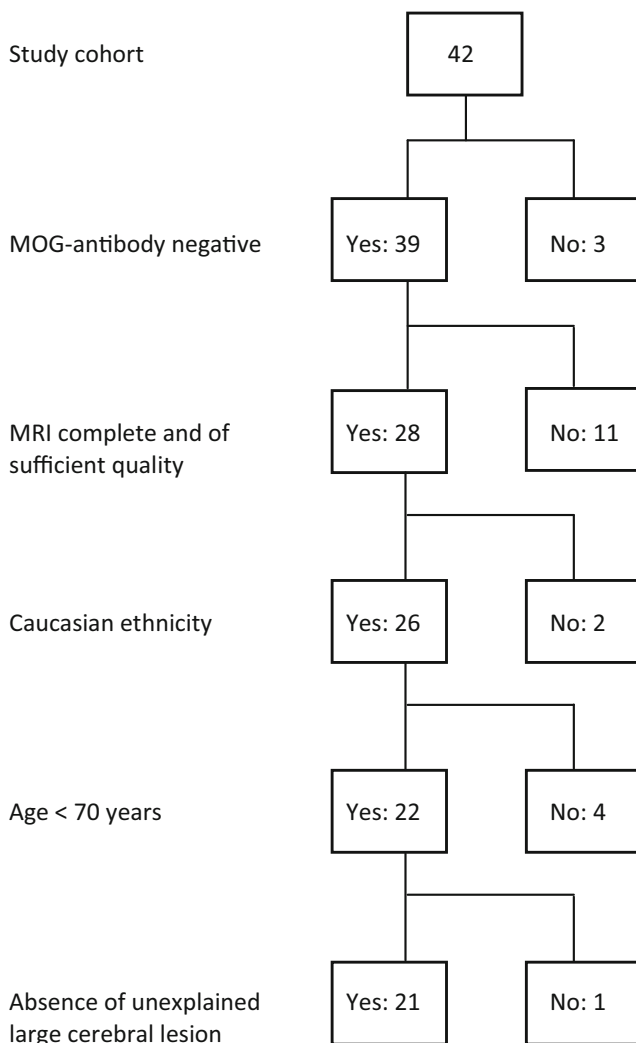


**Fig. 1** Flow chart for inclusion and exclusion of the NMOSD patient cohort.

thickness 1 mm), a volumetric high-resolution T2 weighted sequence (3D SPACE TR/TE=5000/502 ms), a volumetric high-resolution fluid attenuated inversion recovery (3D FLAIR) sequence (TR/TE/TI=6000/388/2100 ms) and a single-shot echo planar imaging DTI sequence (TR / TE=7500/86 ms; FOV=240 x 240 mm<sup>2</sup>; matrix 96×96, 61 slices no gap, slice thickness 2.3 mm, 64 non-colinear directions, b-value=1000 s/mm<sup>2</sup>, one b<sub>0</sub>-volume). T2 hyperintense lesions were manually segmented by a technician (with 5 years experience in lesion definition) on the 3D T2 images in conjunction with 3D FLAIR images.

### MRI—data post-processing

1. *Voxel based morphometry (VBM)*: The manually segmented T2 lesion masks were co-registered to the MPRAGE and lesions were masked out before VBM analysis. The toolbox VBM8 (<http://dbm.neuro.uni-jena.de/vbm>) in combination with SPM8 (<http://www.fil.ion.ucl.ac.uk/spm/software/spm8>.) running under Matlab R2012b (<http://www.mathworks.com>) was used for grey and white matter segmentation including Diffeomorphic Anatomical Registration Through Exponentiated Lie Algebra (DARTEL) normalization and registration [50] (statistical analysis see below).

2. *Subcortical volume and cortical thickness analysis (Freesurfer)*: For segmentation and estimation of subcortical volume and cortical thickness Freesurfer image analysis software v5.3 (<http://surfer.nmr.mgh.harvard.edu>) was used. All data sets were manually controlled, and when necessary, corrected for segmentation errors of the automatic routine. For further analysis, we globally extracted subcortical volume and cortical thickness estimates for lobes and for individual regions (Desikan-Killiany Atlas). The technical details are described in prior publications [51–53], and have previously been applied in NMOSD studies [10, 20]. For a detailed description of the Freesurfer processing stream, please see Fischl [54].
3. *Diffusion Tensor Imaging*: DTI data was processed with tools from the FMRIB Software Library (FSL 5.0.9) [55]. Processing included brain extraction, motion, eddy current distortion correction and a linear tensor model fit that generated maps of fractional anisotropy (FA), mean diffusivity (MD), parallel diffusivity (PD, i.e. the first eigenvalue) and radial diffusivity (RD, i.e. the mean of second and third eigenvalue). All parameter maps were further analyzed in a Tract Based Spatial Statistic (TBSS) analysis. For a detailed description of the TBSS steps and procedure, please see Smith et al. [56]. Influence of lesions on TBSS results were controlled as follows. T2 lesion masks were initially co-registered to the b<sub>0</sub>-volume, and subsequently, non-linear to the TBSS skeleton space. Lesion voxels were excluded from the final analysis with separate script that is provided in FSL (“setup\_masks”—for more information, see <http://fsl.fmrib.ox.ac.uk/fsl/fslwiki/Randomise/UserGuide>).

For an additional region-of-interest (ROI) approach, we combined masks from the Johns-Hopkins University (JHU) DTI-based white-matter atlases with the TBSS skeleton. The intersection of each atlas mask with the TBSS skeleton was used as an ROI for specific tracts. From each tract mask, we extracted the mean FA value for each region and subject.

### Optical coherence tomography

For an evaluation of potential brain damage related to a history of ON, we measured retinal nerve fibre layer thickness (RNFL) in all patients and controls with optical coherence tomography (Spectralis SD-OCT Heidelberg Engineering,

Heidelberg, Germany) in undilated eyes. Peripapillary RNFL thickness was measured using a 3.4 mm ring scan around the optic nerve head with the standard device protocol [57]. All scans passed image quality assessment using the OSCAR-IB criteria [58].

### Statistical analysis

Group differences in gender (Fisher exact test), lesion count and lesion volume (unpaired *t*-test) were compared between groups with the software Graphpad Prism (Version 6.0, GraphPad Software, La Jolla California USA, [www.graphpad.com](http://www.graphpad.com)). VBM and TBSS statistical between-group analysis was performed with the randomise tool (part of FSL) that uses a permutation-based, threshold-free cluster-detection algorithm (TFCE). All analyses were performed with 5000 permutations. TFCE provides an objective method for cluster detection in comparison to often arbitrarily set cluster size definitions that can have a great impact on results [59]. We analyzed group differences (age and gender included as covariates). After significant group differences in the DTI analysis, we tested for a correlation with EDSS and disease duration.

In the light of the heterogeneity in previous studies that used different (strict or exploratory) statistical thresholds, we generated statistical maps at three different statistical thresholds ( $p < 0.05$  and  $p < 0.01$  uncorrected for multiple comparisons, and  $p < 0.05$  family wise error (FWE) corrected for multiple comparisons). We chose this approach to allow for an assessment at different sensitivity and specificity levels across the whole brain and for comparison with previous studies that used these thresholds [15, 16, 20].

Between group differences in subcortical volume measures, cortical thickness and DTI parameter from the combined TBSS JHU atlas mask analysis were analyzed in a linear model (age and gender included as covariates) using the statistical software package R project (R 3.1.0 <http://www.r-project.org>).

**Table 1** Demographic data of controls and NMOSD patient cohort, EDSS = Expanded disability status scale, AQP = Aquaporin, ON = optic neuritis, LETM = longitudinal extensive transverse myelitis, NA = not applicable

	Controls	NMOSD	<i>p</i> value
Subject (n)	21	21	–
Gender (f/m)	18 / 3	18 / 3	1.0
Age in years (mean ± sd)	44.8 ± 14.9	44.7 ± 12.8	0.97
AQP-4 IgG + (n)		19/21	–
Disease duration months (mean ± sd)	NA	111.7 (±121.4)	–
EDSS median (range)	NA	3.8 (1.0– 6.0)	–
ON status no / unilat / both eyes	NA	2 / 12 / 7	–
LETM status (no / yes)	NA	2 / 19	–
T2 lesion count (mean ± sd)	6.0 ± 7.7	15.5 ± 22.7	0.08
T2 lesion volume in ml (mean ± sd)	0.19 ± 0.31	0.78 ± 1.10	0.02

Finally, we evaluated ON associated degeneration in the optic radiation in a generalized estimating equation model (GEE – r package *geepack* 1.2.0 [60]). GEE was used to account for intra-patient/inter-eye effects (age and gender included as covariates). Based on the DTI results (see below), we tested only for an association between RNFL values and FA values within the optic radiation. For this analysis, we used FA values from the optic radiation that were extracted from the JHU atlas mask approach.

## Results

### Study participants

We analyzed 21 NMOSD patients and 21 healthy control subjects.

Almost all patients (19/21) were positive for AQP IgG. The two patients that were negatively tested both fulfilled the Wingerchuck 2006 and 2015 criteria [30, 31].

Patient and control groups did not differ in age ( $p = 0.98$ ) or gender ( $p = 1.0$ ; Table 1). Two patients did not receive medication on a regular basis (one patient due to stable seronegative disease and one patient due to persistent idiopathic leukopenia). The majority of patients were under immunosuppressive therapy—either azathioprine, rituximab, cyclophosphamide, methotrexate, mycophenolate mofetil or intermittent plasma exchange.

The majority (17/21) of NMOSD patients (17/21) and control subjects (14/21) had T2 WM lesions (Fisher exact test  $p$  value = 0.27). Lesion volume was significantly higher in NMOSD patients ( $p = 0.02$ ) and a trend towards higher lesion count ( $p = 0.08$ ) was observed.

### Voxel-based morphometry

At liberal “exploratory” statistical threshold, various regions showed a significant GW and WM volume decrease in



patients, e.g. in the frontobasal cortex, insular cortex, occipital cortex and cerebellum. However, after correction for multiple comparisons, no significant differences between NMOSD and controls remained. No regions showed a GM or WM volume increase in patients.

### Freesurfer analysis

We did not find statistically significant differences in subcortical volume or cortical thickness between NMOSD patients and controls (see Table 2 and Suppl. Table 1 for a detailed gyri-based cortical thickness analysis) (Fig 2).

### Diffusion tensor imaging—TBSS

Significant FA reductions (Fig. 3) at a conservative statistical threshold ( $p < 0.05$  corrected for multiple comparisons) could be demonstrated only in the optic radiation; these were driven by RD increases (Suppl. Fig. 1). PD and MD did not demonstrate significant differences between NMOSD patients and controls at conservative statistical thresholds (Suppl. Fig. 1). Also, at lower statistical thresholds, other regions demonstrate FA reductions (with associated RD and MD increases), e.g. corticospinal tract, splenium, corpus callosum genu, corpus callosum body, cerebellum and brainstem (Fig. 3). However, no association with EDSS or disease duration could be demonstrated (data not shown).

**Table 2** Freesurfer results (mean  $\pm$  sd) of subcortical volume (in  $\text{cm}^3$ ) and cortical thickness (in mm)

Volume	Controls	Patients	<i>p</i> value
Total GM Volume	611.8 $\pm$ 46.31	602.95 $\pm$ 58.66	0.59
Cortical Volume	430.01 $\pm$ 35.37	425.00 $\pm$ 44.32	0.69
Subcortical GM Volume	181.79 $\pm$ 13.39	177.95 $\pm$ 16.56	0.41
Intracranial Volume	1293.27 $\pm$ 207.4	1292.11 $\pm$ 236.03	0.99
Thalamus	6.90 $\pm$ 0.71	6.76 $\pm$ 0.72	0.51
Caudate	3.40 $\pm$ 0.45	3.36 $\pm$ 0.41	0.79
Putamen	4.96 $\pm$ 0.47	4.89 $\pm$ 0.66	0.69
Pallidum	1.58 $\pm$ 0.11	1.57 $\pm$ 0.19	0.83
Hippocampus	4.18 $\pm$ 0.33	4.31 $\pm$ 0.36	0.24
Amygdala	1.55 $\pm$ 0.15	1.60 $\pm$ 0.17	0.29
Cortical thickness	Controls	Patients	<i>p</i> value
Frontal	2.56 $\pm$ 0.09	2.55 $\pm$ 0.12	0.75
Cingulate	2.71 $\pm$ 0.11	2.63 $\pm$ 0.15	0.09
Occipital	1.97 $\pm$ 0.07	1.96 $\pm$ 0.12	0.58
Postcentral	2.08 $\pm$ 0.12	2.02 $\pm$ 0.15	0.20
Precentral	2.58 $\pm$ 0.11	2.52 $\pm$ 0.18	0.21
Temporal	2.80 $\pm$ 0.09	2.79 $\pm$ 0.14	0.80
Parietal	2.39 $\pm$ 0.09	2.37 $\pm$ 0.15	0.62
Insula	3.09 $\pm$ 0.14	3.06 $\pm$ 0.18	0.55

### Diffusion tensor imaging - TBSS-JHU atlas

In the additional ROI approach with a combined TBSS-JHU atlas mask analysis, significant FA reductions were found exclusively in regions of the occipital lobe (Suppl. Table 2). All of these regions are part of (posterior thalamic radiation  $p < 0.001$ , 6.9 % difference), in the immediate vicinity (sagittal stratum  $p < 0.003$ , 5.6 % difference; tapetum  $p < 0.019$ , 7.1 % difference) or functionally directly connected (splenium  $p < 0.039$ , 2.6 % difference) to the visual system. Note that the cerebral peduncle as part of the cortical spinal tract just misses statistical significance ( $p$  value = 0.052, 1.4 % difference).

### Association of RNFL and FA in the optic radiation

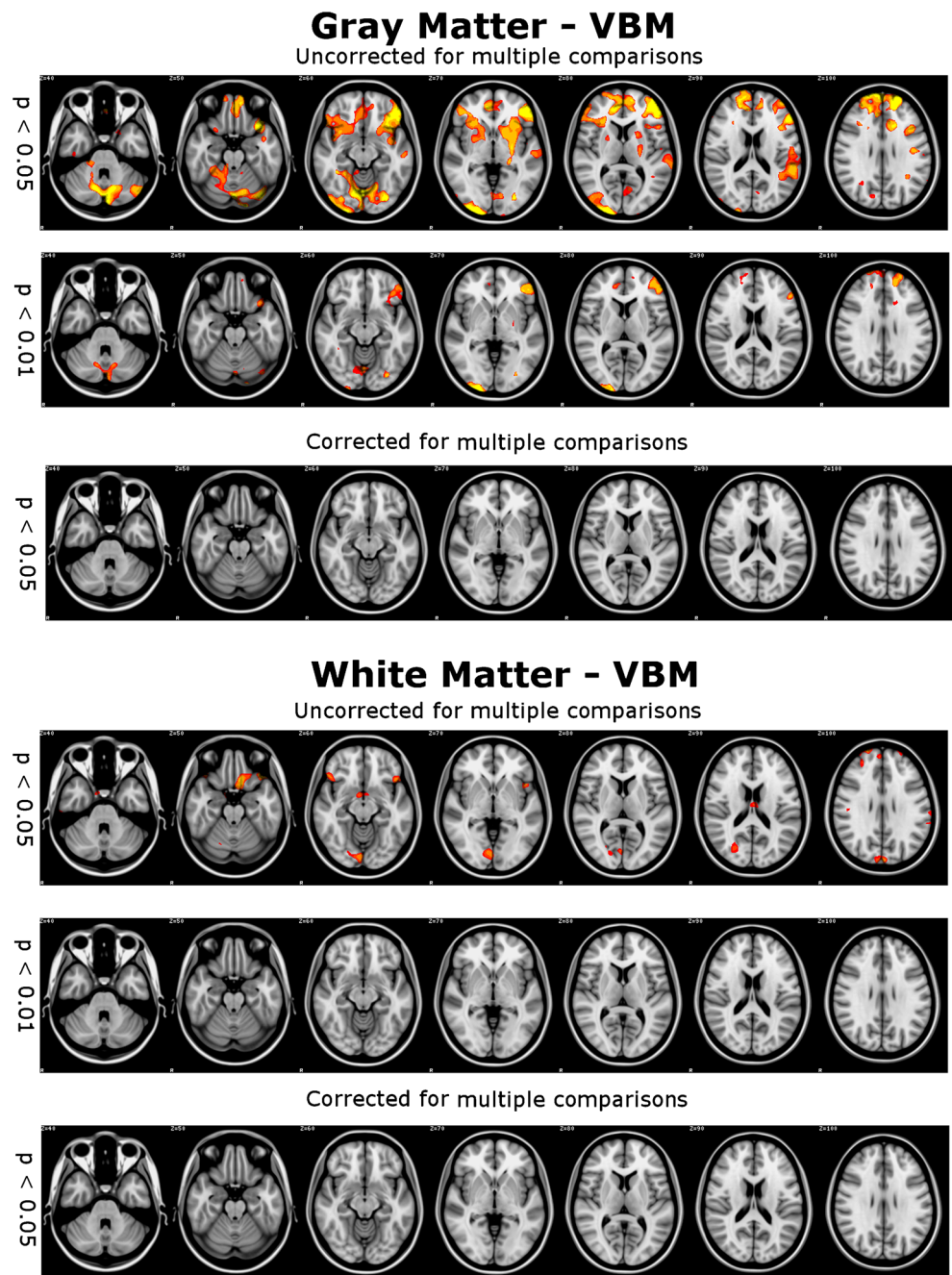
Mean RNFL values (overall, nasal and temporal quadrants) were significantly different ( $p < 0.001$ ) between NMOSD patients (mean  $\pm$  sd = 74.6  $\pm$  17.0 mm) and controls (mean  $\pm$  sd = 98.3  $\pm$  6.9 mm). The GEE analysis showed a significant association ( $p = 0.038$ ) between RNFL and FA values in the optic radiation with lower RNFL values reflecting reduced FA in the optic radiation.

### Discussion

Our study investigated if occult brain parenchymal damage in NMOSD patients can be detected using a multiparametric MRI approach. In the past decade, especially with identification of anti-AQP4 antibodies, the understanding of NMOSD has dramatically changed [1]. However, prevalence and pathogenesis of brain involvement in NMOSD (in addition to the hallmark symptoms ON and LETM) is still a matter of debate. Nonspecific white matter abnormalities are found in a relatively high percentage (30–80 %) of NMOSD patients [1, 33]. Also in our cohort, the majority of patients (17/21) had smaller unspecific white matter lesions. This relatively high percentage can be explained with the greater sensitivity of lesion detection in the 3D high-resolution (1 mm isotropic) T2 and FLAIR sequences that were used in our protocol. This is also reflected by the high percentage (14/21) of control subjects with white matter lesions. Nonetheless, T2 lesion volume was higher in NMOSD patients and further studies with high-resolution T2 imaging and other techniques (e.g. susceptibility weighted imaging) to characterize these lesions are warranted.

Various advanced MRI techniques (H-MRS, MTI, DTI, VBM, CTA) have been used in the past to investigate NMOSD occult brain parenchymal damage, with most studies using one of these techniques. Only two studies previously used a true multimodal approach [15, 20]. Pichiecchio et al. compared H-MRS, MTI, VBM and DTI, while von Glehn et al. [20, 15] compared VBM, CTA and DTI.

**Fig 2** GM and WM VBM results at  $p < 0.05$  and  $p < 0.01$  uncorrected, and  $p < 0.05$  corrected for multiple comparisons. At exploratory statistical threshold different GM and WM regions show significant GM and WM volume decrease in NMOSD patients. After correction for multiple comparisons no significant differences remained

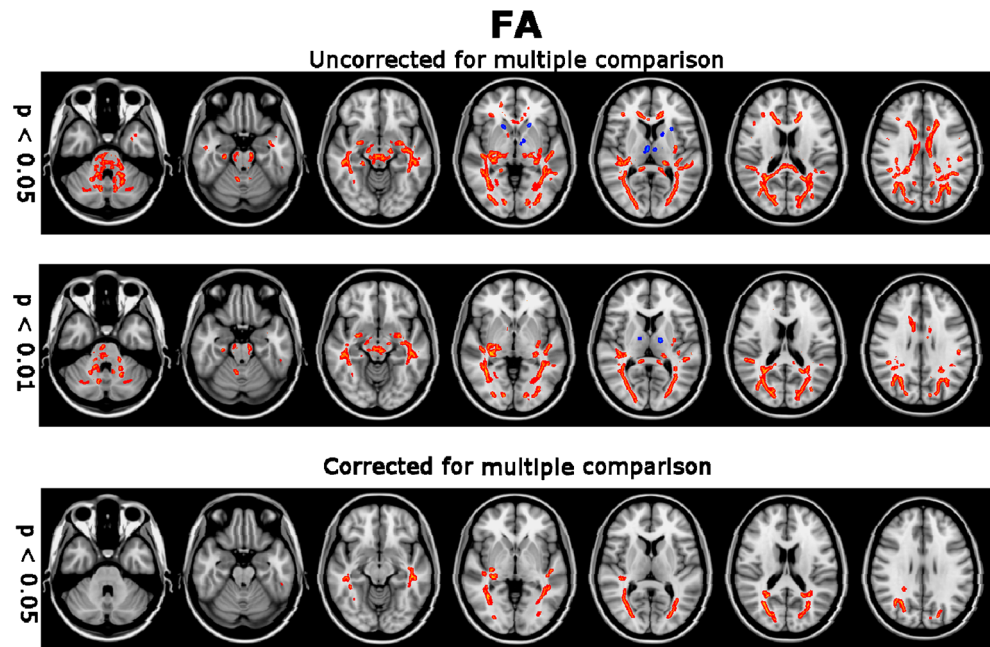


**H-MRS and MTI:** In the study by Pichiecchio et al. H-MRS and MTI did not reveal any significant differences. Also other previous studies that used H-MRS [7–9] and MTI [3, 4, 15] did not find any or only very moderate differences using these techniques.

**Voxel-based morphometry:** Previous VBM studies in NMOSD showed rather conflicting results. In the study by von Glehn et al. [20], GM volumetric reductions for NMO patients compared to healthy control subjects were reported in frontal, parietal, temporal, occipital, limbic and cerebellar

areas. However, identical to our VBM results, these differences were significant only at exploratory thresholds and supposedly not significant after correction for multiple comparisons, which was not reported. Duan et al. [16] also similarly reported GM atrophy in NMO patients across several frontal and temporal regions, but after correction for multiple comparisons, no significant GM atrophy was found. In a follow-up study by the same group [22], significant clusters of reduced WM volume in several frontal, parietal, and occipital brain regions were reported (results were corrected with “AlphaSim

**Fig. 3** TBSS FA differences at  $p < 0.05$  uncorrected and  $p < 0.01$  uncorrected, and  $p < 0.05$  fwe corrected for multiple comparisons. Red-Yellow = reduction in patients / Blue-Light blue = increase in patients. For visualization purposes, significant skeleton tracts are thickened (tbss\_fill script of fs)



programme at  $p < 0.05$  at a voxel level across the whole brain” [22]). In a further study, Blanc et al. [17] also did not find GM volume differences between NMO patients and controls, but reported on focal white matter volume loss in the optic chiasm, pons, cerebellum, the corpus callosum and parts of the frontal, temporal and parietal lobes (false discovery rate correction at  $p < 0.05$ , cluster size threshold 30 voxels). On the contrary, Pichiecchio et al. [15] observed no WM atrophy, but reported on focal GM volume reduction in the sensorimotor and the visual cortex. To address the heterogeneity of statistical thresholds used in previous studies and to allow for an objective and full assessment at different sensitivity and specificity levels, we avoided arbitrary cluster definitions by using the automated TFCE-method for cluster detection, and reported at three different statistical thresholds. Consistent with most of the previous studies at conservative thresholds, no significant volume decreases could be demonstrated; however, at liberal thresholds, several GM and WM regions showed a significant atrophy.

**Subcortical volume and cortical thickness analysis:** The two previous studies using CTA methods also showed rather conflicting results. Von Glehn et al. [20] reported widespread changes in cortical thickness in “almost all cerebral lobes”. Calabrese et al. [10] report on “mild thinning” limited to visual (calcarine gyri) and sensorimotor areas (pre- and postcentral gyrus). In our study, no significant group differences in subcortical volume or cortical thickness were found.

**Diffusion Tensor Imaging:** All previous DTI studies in NMO reported significant differences in normal appearing white matter, with a remarkable consistency across studies, despite differences in DTI post-processing approaches, e.g.

manual ROI, TBSS or tractography. However, some of the studies differ in the extent of the reported white matter damage as discussed above. Diffusion Kurtosis Imaging (DKI), a relatively novel diffusion based method, was compared to DTI in two recent studies by the same group [19, 21], but DKI demonstrated no additional detection sensitivity compared to DTI. The DTI results in our study suggest predominant WM damage in the visual system and the sensorimotor system, while in the latter, only a statistical trend could be demonstrated. This finding is consistent to previous NMOSD DTI studies [5, 6, 11–15, 19–21]. The majority of studies are in agreement with our findings including that 1) FA decreases are driven by RD increases [44], and 2) that the sensorimotor system is less affected.

The damage in the visual and the sensorimotor system may well be explained by secondary degeneration as a consequence of the two NMOSD hallmark symptoms ON and LETM. This interpretation is corroborated in our study by a significant association between retinal damage caused by previous ON, i.e., RNFL thinning, and a DTI based WM damage assessment in the optic radiation. Similar associations between retinal thinning and damage to the posterior visual pathway have been reported in patients with multiple sclerosis and optic neuritis [61–63]. Moreover, previous studies in NMO reported a positive RNFL thickness correlation to pericalcarine cortical thickness [20] and a correlation between clinical scores and FA values in the visual and the sensorimotor system [6], which we could not find in our study.

In addition to the hypothesis of a secondary degeneration as a consequence to ON and LETM, a different damaging mechanism in NMOSD needs to be discussed. The cellular target of NMOSD inflammation is the AQP-4 water channel antigen



located in astrocytic endfeet processes and expressed across the whole brain and spinal cord [26]. In periventricular areas with high AQP-4 expression, demyelinating lesions and characteristic MRI lesions have been described [39, 40], and some of the previous DTI imaging studies [11, 14, 20, 21] reported damage in white matter tracts beyond the visual and the sensorimotor system. However, the hypothesis of a primary and widespread brain parenchymal damage in NMOSD has been recently challenged by a histopathological study that demonstrates lack of a relevant cortical pathology in NMOSD [34], including a normal cortical AQP-4 distribution [64]. The reported widespread abnormalities in the DTI studies mentioned above may also be explained by competing effects that are only indirectly related to NMOSD pathology. Several studies in other groups of chronically ill patients on aggressive immunosuppressive medication, such as patients on chemotherapy, have demonstrated widespread brain structural changes [65]. In addition, considering a usual study design with recruitment of healthy controls will result in exclusion of control subjects suffering from chronic diseases. This results in a “super-healthy” control group. When advanced sensitive methods (e.g. DTI) are applied, “significant differences” will likely appear in many patient populations, especially in elderly, chronically ill patients on polypharmacotherapy.

### Limitations

About half of the initially screened patients were excluded from the study to reduce the heterogeneity of our patient sample (Fig. 1). This in turn might have caused a selection bias. However, the present analyses clearly required a well-defined NMOSD patient cohort, and we therefore minimized confounders such as a mix of different disease entities that would fulfill the NMOSD criteria: e.g. exclusion of MOG antibody positive patients, exclusion of non-Caucasian patients (with regard to possible genetic influence, i.e. Asian optico-spinal MS), and exclusion of patients with unexplained cerebral lesions.

Our study and all previous imaging NMOSD studies are limited in sample size and validation in bigger cohorts is necessary. One possible solution to this difficulty in a rare disease like NMOSD would be to share available data in an international study group and pool imaging data in a common database. This would allow for evaluation of NMOSD brain damage in more detail with enhanced statistical power.

### Conclusion

Our findings together with previous results suggest that NMOSD brain damage not detectable with routine MRI methods can be visualized with advanced MRI techniques. NMOSD specific parenchymal brain damage is consistently

located in the visual and sensorimotor system, and is likely due to a secondary degeneration caused by ON and LETM. Damage outside the two systems appears to be less severe and can potentially be explained by factors other than NMOSD specific pathomechanisms, but needs to be further addressed in larger cohorts. In comparison of different imaging methods, DTI appears to be the most reliable and sensitive technique for brain damage detection in NMOSD.

**Acknowledgments** The scientific guarantor of this publication is Prof. Dr. med. Friedemann Paul. The authors of this manuscript declare no relationships with any companies, whose products or services may be related to the subject matter of the article. This study has received funding from the Bundesministerium für Bildung und Forschung (BMBF Competence Network Multiple Sclerosis to FP, FIP, JW and KR) and by Deutsche Forschungsgemeinschaft (Exc 257 to FP), as well as from BIH-Charité Clinical Scientist Program funded by the Charité-Universitätsmedizin Berlin and the Berlin Institute of Health (to FIP). No complex statistical methods were necessary for this paper. Institutional Review Board approval was obtained.

Written informed consent was obtained from all subjects (patients) in this study. Methodology:

Prospective, cross sectional study, one institution.

### References

1. Kim HJ, Paul F, Lana-Peixoto MA et al (2015) MRI characteristics of neuromyelitis optica spectrum disorder: an international update. *Neurology* 84:1165–1173
2. Jarius S, Wildemann B, Paul F (2014) Neuromyelitis optica: clinical features, immunopathogenesis and treatment. *Clin Exp Immunol* 176:149–164
3. Filippi M, Rocca MA, Momiola L et al (1999) MRI and magnetization transfer imaging changes in the brain and cervical cord of patients with Devic's neuromyelitis optica. *Neurology* 53: 1705–1705
4. Rocca MA, Agosta F, Mezzapesa DM et al (2004) Magnetization transfer and diffusion tensor MRI show gray matter damage in neuromyelitis optica. *Neurology* 62:476–478
5. Yu CS, Lin FC, Li KC et al (2006) Diffusion tensor imaging in the assessment of normal-appearing brain tissue damage in relapsing neuromyelitis optica. *AJNR Am J Neuroradiol* 27:1009–1015
6. Yu C, Lin F, Li K et al (2008) Pathogenesis of Normal-appearing White Matter Damage in Neuromyelitis Optica: Diffusion-Tensor MR Imaging. *Radiology* 246:222–228
7. Bichuetti DB, Rivero RLM, de Oliveira EML et al (2008) White matter spectroscopy in neuromyelitis optica: a case control study. *J Neurol* 255:1895–1899
8. Aboul-Enein F, Krssák M, Höftberger R et al (2010) Diffuse white matter damage is absent in neuromyelitis optica. *AJNR Am J Neuroradiol* 31:76–79
9. de Seze J, Blanc F, Kremer S et al (2010) Magnetic resonance spectroscopy evaluation in patients with neuromyelitis optica. *J Neurol Neurosurg Psychiatry* 81:409–411
10. Calabrese M, Oh MS, Favaretto A et al (2012) No MRI evidence of cortical lesions in neuromyelitis optica. *Neurology* 79: 1671–1676
11. Rueda Lopes FC, Doring T, Martins C et al (2012) The Role of Demyelination in Neuromyelitis Optica Damage: Diffusion-Tensor MR Imaging Study. *Radiology* 263:235–242



12. Zhao D-D, Zhou H-Y, Wu Q-Z et al (2012) Diffusion tensor imaging characterization of occult brain damage in relapsing neuromyelitis optica using 3.0T magnetic resonance imaging techniques. *NeuroImage* 59:3173–3177
13. Jeantroux J, Kremer S, Lin XZ et al (2012) Diffusion tensor imaging of normal-appearing white matter in neuromyelitis optica. *J Neuroradiol J Neuroradiol* 39:295–300
14. Liu Y, Duan Y, He Y et al (2012) A tract-based diffusion study of cerebral white matter in neuromyelitis optica reveals widespread pathological alterations. *Mult Scler Houndmills Basingstoke Engl* 18:1013–1021
15. Pichiecchio A, Tavazzi E, Poloni G et al (2012) Advanced magnetic resonance imaging of neuromyelitis optica: a multiparametric approach. *Mult Scler Houndmills Basingstoke Engl* 18:817–824
16. Duan Y, Liu Y, Liang P et al (2012) Comparison of grey matter atrophy between patients with neuromyelitis optica and multiple sclerosis: A voxel-based morphometry study. *Eur J Radiol* 81: e110–e114
17. Blanc F, Noblet V, Jung B et al (2012) White matter atrophy and cognitive dysfunctions in neuromyelitis optica. *PLoS One* 7: e33878
18. Chanson J-B, Lamy J, Rousseau F et al (2013) White matter volume is decreased in the brain of patients with neuromyelitis optica. *Eur J Neurol* 20:361–367
19. Kimura MCG, Doring TM, Rueda FC et al (2014) In vivo assessment of white matter damage in neuromyelitis optica: a diffusion tensor and diffusion kurtosis MR imaging study. *J Neurol Sci* 345: 172–175
20. von Glehn F, Jarius S, Cavalcanti Lira RP et al (2014) Structural brain abnormalities are related to retinal nerve fiber layer thinning and disease duration in neuromyelitis optica spectrum disorders. *Mult Scler*. doi:10.1177/1352458513519838
21. Doring TM, Lopes FCR, Kubo TTA et al (2014) Neuromyelitis optica: a diffusional kurtosis imaging study. *AJNR Am J Neuroradiol* 35:2287–2292
22. Duan Y, Liu Y, Liang P et al (2014) White matter atrophy in brain of neuromyelitis optica: a voxel-based morphometry study. *Acta Radiol* 55:589–593
23. Lopes FCR, Alves-Leon SV, Godoy JM et al (2015) Optic Neuritis and the Visual Pathway: Evaluation of Neuromyelitis Optica Spectrum by Resting-State fMRI and Diffusion Tensor MRI. *J Neuroimaging Off J Am Soc Neuroimaging*. doi:10.1111/jon.12191
24. Kremer S, Renard F, Achard S et al (2015) Use of Advanced Magnetic Resonance Imaging Techniques in Neuromyelitis Optica Spectrum Disorder. *JAMA Neurol* 72:815–822
25. Jarius S, Wildemann B (2013) The history of neuromyelitis optica. *J Neuroinflammation* 10:8
26. Jarius S, Paul F, Franciotta D et al (2008) Mechanisms of disease: aquaporin-4 antibodies in neuromyelitis optica. *Nat Clin Pract Neurol* 4:202–214
27. Lennon VA, Wingerchuk DM, Kryzer TJ et al (2004) A serum autoantibody marker of neuromyelitis optica: distinction from multiple sclerosis. *Lancet* 364:2106–2112
28. Lennon VA, Kryzer TJ, Pittock SJ et al (2005) IgG marker of optic-spinal multiple sclerosis binds to the aquaporin-4 water channel. *J Exp Med* 202:473–477
29. Metz I, Beißbarth T, Ellenberger D et al (2016) Serum peptide reactivities may distinguish neuromyelitis optica subgroups and multiple sclerosis. *Neurol Neuroimmunol Neuroinflamm* 2016;3: e204
30. Wingerchuk DM, Lennon VA, Pittock SJ et al (2006) Revised diagnostic criteria for neuromyelitis optica. *Neurology* 66: 1485–1489
31. Wingerchuk DM, Banwell B, Bennett JL et al (2015) International consensus diagnostic criteria for neuromyelitis optica spectrum disorders. *Neurology* 85:177–189
32. Kister I, Paul F (2015) Pushing the boundaries of neuromyelitis optica: does antibody make the disease? *Neurology* 85:118–119
33. Jarius S, Ruprecht K, Wildemann B et al (2012) Contrasting disease patterns in seropositive and seronegative neuromyelitis optica: A multicentre study of 175 patients. *J Neuroinflammation* 9:14
34. Cabrera-Gómez JA, Quevedo-Sotolongo L, González-Quevedo A et al (2007) Brain magnetic resonance imaging findings in relapsing neuromyelitis optica. *Mult Scler Houndmills Basingstoke Engl* 13: 186–192
35. Li Y, Xie P, Lv F et al (2008) Brain magnetic resonance imaging abnormalities in neuromyelitis optica. *Acta Neurol Scand* 118:218–225
36. Matthews L, Marasco R, Jenkinson M et al (2013) Distinction of seropositive NMO spectrum disorder and MS brain lesion distribution. *Neurology* 80:1330–1337
37. Sinnecker T, Dörr J, Pfueller CF et al (2012) Distinct lesion morphology at 7-T MRI differentiates neuromyelitis optica from multiple sclerosis. *Neurology* 79:708–714
38. Kister I, Herbert J, Zhou Y, Ge Y (2013) Ultrahigh-Field MR (7 T) Imaging of Brain Lesions in Neuromyelitis Optica. *Mult Scler Int* 2013:398259
39. Pittock SJ, Lennon VA, Krecke K et al (2006) Brain abnormalities in neuromyelitis optica. *Arch Neurol* 63:390–396
40. Tackley G, Kuker W, Palace J (2014) Magnetic resonance imaging in neuromyelitis optica. *Mult Scler J* 20:1153–1164
41. Chan K, Tse CT, Chung CP et al (2011) Brain involvement in neuromyelitis optica spectrum disorders. *Arch Neurol* 68:1432–1439
42. He D, Wu Q, Chen X et al (2011) Cognitive impairment and whole brain diffusion in patients with neuromyelitis optica after acute relapse. *Brain Cogn* 77:80–88
43. Rocca MA, Parisi L, Pagani E et al (2014) Regional but not global brain damage contributes to fatigue in multiple sclerosis. *Radiology* 273:511–520
44. Rueda Lopes FC, Doring T, Martins C et al (2012) The Role of Demyelination in Neuromyelitis Optica Damage: Diffusion-Tensor MR Imaging Study. *Radiology* 263:235–242
45. de Seze J, Blanc F, Kremer S et al (2010) Magnetic resonance spectroscopy evaluation in patients with neuromyelitis optica. *J Neurol Neurosurg Psychiatry* 81:409–411
46. Yu CS, Zhu CZ, Li KC et al (2007) Relapsing Neuromyelitis Optica and Relapsing-Remitting Multiple Sclerosis: Differentiation at Diffusion-Tensor MR Imaging of Corpus Callosum 1. *Radiology* 244:249–256
47. Wingerchuk DM, Lennon VA, Lucchinetti CF et al (2007) The spectrum of neuromyelitis optica. *Lancet Neurol* 6:805–815
48. Dalmau J (2015) Observations on the evolving fields of neuroimmunology and neuroinflammation. *Neurol Neuroimmunol Neuroinflammation* 2:e67
49. Kitley J, Leite MI, Nakashima I et al (2012) Prognostic factors and disease course in aquaporin-4 antibody-positive patients with neuromyelitis optica spectrum disorder from the United Kingdom and Japan. *Brain J Neurol* 135:1834–1849
50. Ashburner J (2007) A fast diffeomorphic image registration algorithm. *NeuroImage* 38:95–113
51. Fischl B, Dale AM (2000) Measuring the thickness of the human cerebral cortex from magnetic resonance images. *Proc Natl Acad Sci U S A* 97:11050–11055
52. Desikan RS, Ségonne F, Fischl B et al (2006) An automated labeling system for subdividing the human cerebral cortex on MRI scans into gyral based regions of interest. *NeuroImage* 31:968–980

53. Fischl B, Salat DH, Busa E et al (2002) Whole brain segmentation: automated labeling of neuroanatomical structures in the human brain. *Neuron* 33:341–355
54. Fischl B (2012) FreeSurfer. *NeuroImage* 62:774–781
55. Jenkinson M, Beckmann CF, Behrens TEJ et al (2012) FSL. *NeuroImage* 62:782–790
56. Smith SM, Jenkinson M, Johansen-Berg H et al (2006) Tract-based spatial statistics: voxelwise analysis of multi-subject diffusion data. *NeuroImage* 31:1487–1505
57. Oberwahrenbrock T, Ringelstein M, Jentschke S et al (2013) Retinal ganglion cell and inner plexiform layer thinning in clinically isolated syndrome. *Mult Scler* 19:1887–1895
58. Tewarie P, Balk L, Costello F et al (2012) The OSCAR-IB Consensus Criteria for Retinal OCT Quality Assessment. *PLoS One* 7:e34823
59. Smith SM, Nichols TE (2009) Threshold-free cluster enhancement: addressing problems of smoothing, threshold dependence and localisation in cluster inference. *NeuroImage* 44: 83–98
60. Højsgaard S, Halekoh U, Yan J (2006) The R Package geepack for Generalized Estimating Equations. *J Stat Softw* 15(2):1–11
61. Gabilondo I, Martínez-Lapiscina EH, Fraga-Pumar E et al (2015) Dynamics of retinal injury after acute optic neuritis. *Ann Neurol* 77: 517–528
62. Sinnecker T, Oberwahrenbrock T, Metz I et al (2015) Optic radiation damage in multiple sclerosis is associated with visual dysfunction and retinal thinning—an ultrahigh-field MR pilot study. *Eur Radiol* 25:122–131
63. Pfueller CF, Brandt AU, Schubert F et al (2011) Metabolic changes in the visual cortex are linked to retinal nerve fiber layer thinning in multiple sclerosis. *PLoS One* 6:e18019
64. Popescu BFG, Parisi JE, Cabrera-Gómez JA et al (2010) Absence of cortical demyelination in neuromyelitis optica. *Neurology* 75: 2103–2109
65. Simó M, Rifà-Ros X, Rodríguez-Fornells A, Bruna J (2013) Chemobrain: a systematic review of structural and functional neuroimaging studies. *Neurosci Biobehav Rev* 37:1311–1321